AIAA JOURNAL
Vol. 41, No. 6, June 2003

Numerical Study of Mixing Enhancement by Shock Waves in Model Scramjet Engine

Ji-Ho Kim,* Youngbin Yoon,† and In-Seuck Jeung‡
Seoul National University, Seoul 151-742, Republic of Korea
Hwanil Huh§
Chungnam National University, Daejeon 305-764, Republic of Korea
and
Jeong-Yeol Choi§
Pusan National University, Pusan 609-735, Republic of Korea

A numerical study has been conducted to investigate the effect of shock waves on the supersonic hydrogen–air jet flame stabilized in a Mach 2.5 circular cross-section combustor. The numerical model utilizes multispecies Navier–Stokes equations with detailed chemical reaction models and employs a k–ω shear stress transport model. A wedge is mounted on the side wall of the combustor in order to find the interaction of the oblique shock waves with the hydrogen–air jetlike flame. The interaction between the shock waves and the mixing layer is classified according to the increasing tendency of the growth rate of the mixing layer downstream of the shock waves. It is found that the shock waves create a radially inward/outward airflow to the flame and elongate a flame-holding recirculation zone, and thus fuel–air mixing is enhanced significantly, resulting in improved combustion efficiency. Also, the overall performance is investigated by changing the shock position and considering the mixing/combustion efficiency and total pressure loss in a model scramjet combustor. Because there exists a tradeoff between the enhanced mixing/combustion efficiency and the decreased total pressure recovery, it is suggested that the optimized shock position needs to be determined in order to obtain the maximum overall combustor performance using the overall performance index.

Nomenclature

d_F	=	diameter of fuel nozzle lip
I_{op}	=	overall performance index
k	=	turbulent kinetic energy per mass
M	=	Mach number
P	=	pressure
$P_{0,\text{rec}}$	=	total pressure recovery
U	=	velocity
x_W	=	position of leading edge's wedge
Y_{H2}	=	mass fraction of hydrogen
δ_c	=	mixing layer thickness (based on fuel mass fraction)
δ_c'	=	growth rate of mixing layer thickness ($= \partial\delta_c/\partial x$)
η_c	=	combustion efficiency
η_m	=	mixing efficiency
Π	=	total pressure loss
ϕ	=	equivalence ratio

Introduction

IN scramjet engines, combustion occurs at supersonic speeds within a very short residence time of the order of 1 ms, and two issues are essential for efficient operation: the maximization of rapid fuel–air mixing and the minimization of total pressure losses. Unfortunately, shock waves are often unavoidable in a scramjet combustor. However, when the shock waves are sufficiently oblique to the flow, the total pressure losses are not appreciable. Thus, oblique shock waves may have positive effects in enhancing fuel–air mixing and stabilizing the flame.

One of the pronounced effects of shock waves on fuel–air mixing has been identified by Marble et al.[1] They showed that the baroclinic torque creates shock-generated vorticity, enhancing fuel–air mixing. Lu and Wu[2] rigorously studied mixing enhancement of confined supersonic mixing flows by shock waves. They reported that the mixing enhancement using shock waves might be effective if the stimulation by shock waves is spatially continuous and begins very far upstream. Drummond and Givi[3] showed that mixing and combustion efficiencies are extremely low in supersonic flows if the flow is not disturbed by shock waves. Also, Huh and Driscoll[4] reported that shock waves enhance fuel–air mixing and improve the flame stability limit substantially when optimum oblique shock waves are introduced in a supersonic jetlike flame. However, there exists a tradeoff in supersonic flows between the mixing enhancement and the total pressure recovery. From this point of view, they observed only the mixedness using the flame length and did not consider the total pressure loss of a model scramjet combustor simultaneously.[4]

Hence, a new parameter is introduced in the present study: overall performance parameter, which includes both the thrust efficiency and the combustion efficiency. Thrust efficiency is a measure of the total pressure recovery associated with a given heat release due to the combustion, whereas combustion efficiency is simply a measure of the degree of the completeness in mixing and subsequent heat-release processes; i.e., the combustion efficiency may represent only a part of the overall performance. Therefore, the objectives of the present work are to quantify the mixing enhancement and pressure losses using shock waves and to improve the understanding of the mixing enhancement mechanism, which helps to determine the optimized location of shock waves in order to achieve the best performance of a model scramjet engine.

Received 9 October 2001; revision received 24 October 2002; accepted for publication 30 January 2003.

*Graduate Research Assistant, School of Mechanical and Aerospace Engineering. Student Member AIAA.
†Associate Professor, School of Mechanical and Aerospace Engineering; ybyoon@snu.ac.kr. Member AIAA.
‡Professor, School of Mechanical and Aerospace Engineering; enjis@snu.ac.kr. Associate Fellow AIAA.
§Assistant Professor, Department of Aerospace Engineering. Member AIAA.

Numerical Methods

Governing Equations and Numerical Methods

The axisymmetric Navier–Stokes equation for multispecies is employed to analyze a chemically reacting supersonic viscous flow in a supersonic model combustor. The conservation form of these governing equation sets including N number of species is written as follows:

$$\frac{\partial \boldsymbol{Q}}{\partial t}+\frac{\partial \boldsymbol{F}}{\partial x}+\frac{\partial \boldsymbol{G}}{\partial y}+\boldsymbol{H}=\frac{\partial \boldsymbol{F}_v}{\partial x}+\frac{\partial \boldsymbol{G}_v}{\partial y}+\boldsymbol{H}_v+\boldsymbol{W} \tag{1}$$

Conservative variable $\boldsymbol{Q}$; convective flux $\boldsymbol{F}$, $\boldsymbol{G}$; diffusion flux $\boldsymbol{F}_v$, $\boldsymbol{G}_v$; axisymmetric source term $\boldsymbol{H}$, $\boldsymbol{H}_v$; and reaction source term $\boldsymbol{W}$ are defined as follows:

$$\boldsymbol{Q}=\begin{bmatrix}\rho_1\\ \vdots\\ \rho_N\\ \rho u\\ \rho v\\ e\\ \rho k\\ \rho\omega\end{bmatrix},\qquad \boldsymbol{F}=\begin{bmatrix}\rho_1 u\\ \vdots\\ \rho_N u\\ \rho u^2+p\\ \rho uv\\ (e+p)u\\ \rho uk\\ \rho u\omega\end{bmatrix}$$

$$\boldsymbol{G}=\begin{bmatrix}\rho_1 v\\ \vdots\\ \rho_N v\\ \rho uv\\ \rho v^2+p\\ (e+p)v\\ \rho vk\\ \rho v\omega\end{bmatrix},\qquad \boldsymbol{H}=\frac{1}{y}\begin{bmatrix}\rho_1 v\\ \vdots\\ \rho_N v\\ \rho uv\\ \rho v^2\\ (e+p)v\\ \rho vk\\ \rho v\omega\end{bmatrix} \tag{2a}$$

$$\boldsymbol{F}_v=\begin{bmatrix}-\rho_1 u_1^d\\ \vdots\\ -\rho_N u_N^d\\ \tau_{xx}\\ \tau_{xy}\\ \beta_x\\ \dfrac{\mu_k\partial k}{\partial x}\\ \dfrac{\mu_\omega\partial\omega}{\partial x}\end{bmatrix},\qquad \boldsymbol{G}_v=\begin{bmatrix}-\rho_1 v_1^d\\ \vdots\\ -\rho_N v_N^d\\ \tau_{xy}\\ \tau_{yy}\\ \beta_y\\ \dfrac{\mu_k\partial k}{\partial y}\\ \dfrac{\mu_\omega\partial\omega}{\partial y}\end{bmatrix}$$

$$\boldsymbol{H}_v=\frac{1}{y}\begin{bmatrix}-\rho_1 v_1^d\\ \vdots\\ -\rho_N v_N^d\\ \tau_{xy}\\ \tau_{yy}-\tau_{\theta\theta}\\ \beta_y\\ \dfrac{\mu_k\partial k}{\partial y}\\ \dfrac{\mu_\omega\partial\omega}{\partial y}\end{bmatrix},\qquad \boldsymbol{W}=\begin{bmatrix}w_1\\ \vdots\\ w_N\\ 0\\ 0\\ 0\\ S_1\\ S_2\end{bmatrix} \tag{2b}$$

Details of the governing equations and thermal properties are described in a previous paper.[5] Roe's flux difference splitting (FDS) method and the MUSCL scheme are formulated for multispecies with convection flux terms. Diffusion flux terms are discretized by the central difference scheme. The lower–upper–symmetric Gauss Seidel (LU–SGS) method is used as a fully implicit time integration method for the analysis of supersonic reacting flows. The numerical algorithm used in this study has been validated with experimental cases, such as shock-induced combustion phenomena around a blunt body and shock/boundary-layer interaction problems.[6,7]

Chemistry Model and Turbulence Model

The finite rate chemistry model used in the present study consists of 18 steps of chemical reactions with eight reacting species (H, H_2, O, O_2, H_2O, OH, H_2O_2, and HO_2). The reaction data are taken from Jachimowski's 33 detailed chemistry mechanisms for hydrogen–air combustion.[8] Jachimowski's original mechanism includes the oxidation process of nitrogen. However, nitrogen is assumed as an inert gas in this study so that the reaction steps are neglected because the oxidation process does not have a significant effect on the fluid dynamics in a combustor.

Menter's shear stress transport (SST) model[9] is used as a turbulent model. This model is the blending of the standard k–ε model that is suitable for a shear layer problem and Wilcox's k–ω model[10] that is suitable for the wall turbulence effect. Bardina et al.[11] reported that the SST model shows good prediction for mixing layer and jet flow problems, and it is also less sensitive to initial values.

We validated our code with the experimental data of Evans and Schexnayder.[12] They performed experiments and numerical simulations; Mach 2.0 hydrogen fuel was injected into a Mach 1.9 airflow, and vitiated air was used to match it with high enthalpy conditions. Our numerical results have a good agreement with experimental data. To write this paper concisely, we did not include the figures for code validation. Also, this code was used for the previous researches for the model scramjet engine.[13,14]

Model Scramjet Combustor

A schematic of the model scramjet combustor appears in Fig. 1. The specific configurations and conditions of the combustor are similar to those of experiments performed by Huh and Driscoll.[4] However, an axisymmetric configuration is adopted in this study. A hydrogen fuel jet is injected at a sonic speed with the Mach 2.5 air flow using a thick-lip fuel nozzle, which acts as a bluff body. The combustor is 27.3 cm long, and its radial diameter is 5.7 cm at the fuel injection location. The inner diameter of the fuel nozzle d_F is 0.7 cm, and the outer diameter is 2.54 cm; thus, the nozzle lip thickness H is 0.92 cm. The divergence angle of the combustor sidewalls is 4 deg from the flow axis in order to prevent thermal choking.[15]

The wedges are mounted on the diverging sidewalls as shown in Fig. 1 in order to investigate the effect of shock waves. The angle of the wedge is 10 deg to the side-walls, and the leading edge location of the wedge is varied from 0 to $8d_F$ downstream of the fuel injection plane. Hydrogen is injected at a sonic speed. Air is injected at the Mach number of 2.5, where the static temperature is 888 K and static pressure is 0.80 atm, as shown in Table 1. These conditions

Table 1 Initial conditions in a model scramjet combustor

Component	M	U, m/s	T, K	P, atm
Fuel	1.0	1192	245	1.12
Air	2.5	1353	888	0.80

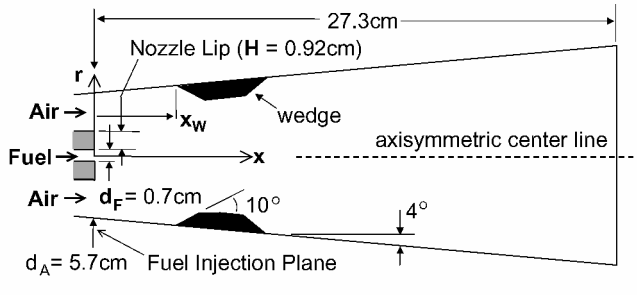

Fig. 1 Schematic of a model scramjet combustor and inflow conditions.

correspond to the combustor inlet flow conditions of Mach 6.0 supersonic flight at the altitude of 26 km from sea level, where the atmospheric temperature is 223 K and pressure is 0.02 atm.

The shape of the wedge used in this simulation slightly differs from that of the experiment of Huh and Driscoll.[4] The former has the slanted shape at both sides, and the latter has the shape of the backward step in the aft part. However, the flowfields have very similar pattterns because a recirculation zone is made behind the backward step wedge and acts as a solid body, like a slanted wall. Although the slanted wedges were used for computational convenience, reasonable data can be acquired.

The inflow condition with turbulent boundary layers is calculated in advance, and then the main calculation is performed with the obtained inflow condition upstream of the combustor. Therefore, the turbulent boundary-layer profile is taken into account partially for the incoming flows.

The no-slip condition is used around the boundary of the nozzle lip, but the slip condition is used at the combustor wall boundary. This slip boundary condition has advantages in computational convenience because the slip condition requires fewer grids at the wall boundary than the no-slip condition and the shock wave is not smeared in a lower grid resolution. Thus, in the case of this slip wall condition, the grid independency can be acquired at a lower grid resolution than in the case of the no-slip wall condition.

We know that the interaction between thin boundary layers and shock waves should be crucial to resolve the phenomena near the supersonic combustor walls. However, the reason we used the slip boundary condition in the present study is that wall boundary layers do not affect the interaction of shock waves and mixing layers significantly because this interaction occurs in the middle of the combustor rather than near the wall.

In this simulation, the resolution of the grid is 200×100. The grid independency was tested with finer grid sizes, and the present grid size is believed to be fine enough to resolve qualitative trends without losing the detailed information obtained with the finer grid sizes.

Results and Discussion

Flow Characteristics

Figure 2 shows the comparison of a numerical result with an experimental result of Huh and Driscoll.[4] The wedges are located at $4d_F$ from the fuel nozzle. The inlet Mach numbers of air and fuel are 2.5 and 1.0, respectively. The general trends of shock wave patterns obtained from the numerical simulation in Fig. 2b are similar to the experimental observation in Fig. 2a. However, there is a minor difference between the numerical and experimental results because

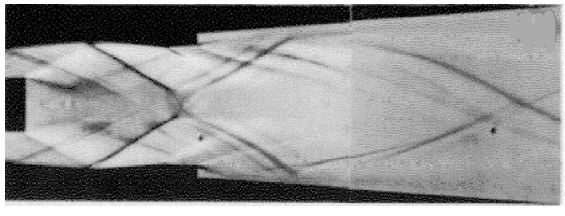

a)

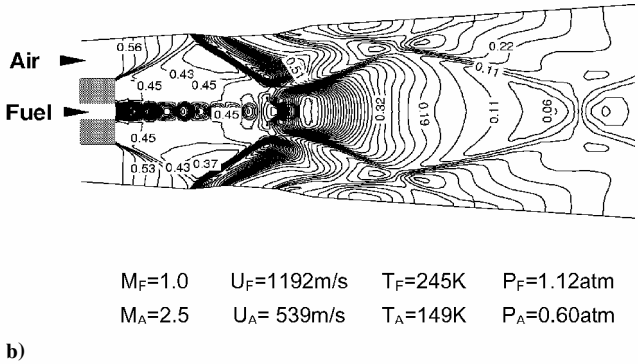

b)

Fig. 2 Nonreacting flow: a) schlieren photograph by Huh and Driscoll[14] and b) pressure contours obtained from the simulation.

of the axisymmetric geometry adopted in the present simulation even though the experiment was performed in the three-dimensional combustor. It is observed that expansion waves occur at the nozzle lip due to the sudden increase in the area. Oblique shocks begin to appear at the leading edge of the wedge. Recompression shock waves are generated by the interaction of the boundary layer and reflected shock waves.

Figure 3 shows pressure, Mach number, mass fraction of hydrogen Y_{H2}, and turbulent kinetic energy contours when a chemical reaction occurs at the initial conditions shown in Fig. 1. In the case with shock waves, the wedge is located at $x/d_F = 4$ from the nozzle. "Shock" indicates the wedge-mounted wall, which makes strong shock waves, whereas "No shock" means the straight wall, which does not generate artificial oblique shock waves but inevitably has innate weak shock waves. The shock waves due to the wedge are expected to create a radially inward/outward airflow to the flame, additional vorticity, and an adverse pressure gradient.[4] Hence, the air entrainment rate and the mixing rate are enhanced near the flame base.

It is noted from Figs. 3a and 3b that pressure in this combustor is increased by the shock waves. However, the Mach number is decreased due to the shock waves resulting in the increment of subsonic regions behind the bluff-body fuel nozzle, as shown in Figs. 3c and 3d. The fuel mass fraction contours in Figs. 3e and 3f illustrate that fuel consumption is significantly increased near the fuel nozzle using the shock waves. The turbulent kinetic energy k contours in Figs. 3g and 3h show the increased values and the broad distribution of turbulence by the shock waves, where k is defined as follows:

$$k = \tfrac{1}{2}\overline{u_i' u_i'} = \tfrac{1}{2}\left(\overline{u'^2} + \overline{v'^2} + \overline{w'^2}\right) \tag{3}$$

The values of turbulent kinetic energy k in Figs. 3g and 3f are nondimensionalized by the square of the sonic velocity a_∞^2.

Figure 3 indicates that strong compression shock waves play an important role in improving the mixing condition by intensifying the turbulence fluctuations through the acceleration of energy extraction from the mean flow, as mentioned by Lu and Wu.[2]

Recirculation Zones

Flame stabilization is an important issue in supersonic combustion. This can be achieved by using a bluff-body fuel nozzle, which provides the flame holding recirculation zone downstream of the fuel nozzle. A flame can be stabilized when the local flow velocity is equal to the normal flame propagation velocity at some points within low-speed recirculation zones. The bluff-body stabilized flame has two counter-rotating recirculation zones; the inner recirculation zone is driven by the fuel jet, and the other zone has recirculation in the opposite direction and is driven by the air flow. It is reported that a reasonable size of recirculation zones is required to stabilize flames in supersonic flows.[16]

The effect of shock waves on the size of the recirculation zone is shown in Fig. 4. When the fuel is ignited, the size of recirculation zones is elongated by about a factor of two compared to the nonreacting case. This may be attributed to the volumetric expansion of highly mixed flow behind the bluff body due to the elevated temperature in the recirculation zone as a result of heat release. Also, it is found that the shock waves further increase the recirculation zone size, which is believed to be due to the strong adverse pressure gradient caused by the shock wave near the recirculation zone.[4] However, when the shock wave is generated at the downstream position ($x_w/d_F = 8$) in the reacting case, the size of the recirculation zone is not affected by shock waves because there is no way to affect the upstream in the flowfield with $M > 1.0$. But in the case of $x_w/d_F = 4$, the recirculation size is affected by the shock waves. This can be explained by the Mach pocket that is shown in Fig. 3d; the Mach number inside of the Mach pocket is not supersonic (i.e., less than 1.0), so that the shock could influence the recirculation zone that is located upstream of shock waves. In the nonreacting case, the size of the recirculation zone is not changed for the case of $x/d_F > 2$. The recirculation zone size is maximized when the wedge is located around $x/d_F = 2$ in the reacting case. This elongated recirculation zone is known to stabilize the supersonic flame more effectively.[17]

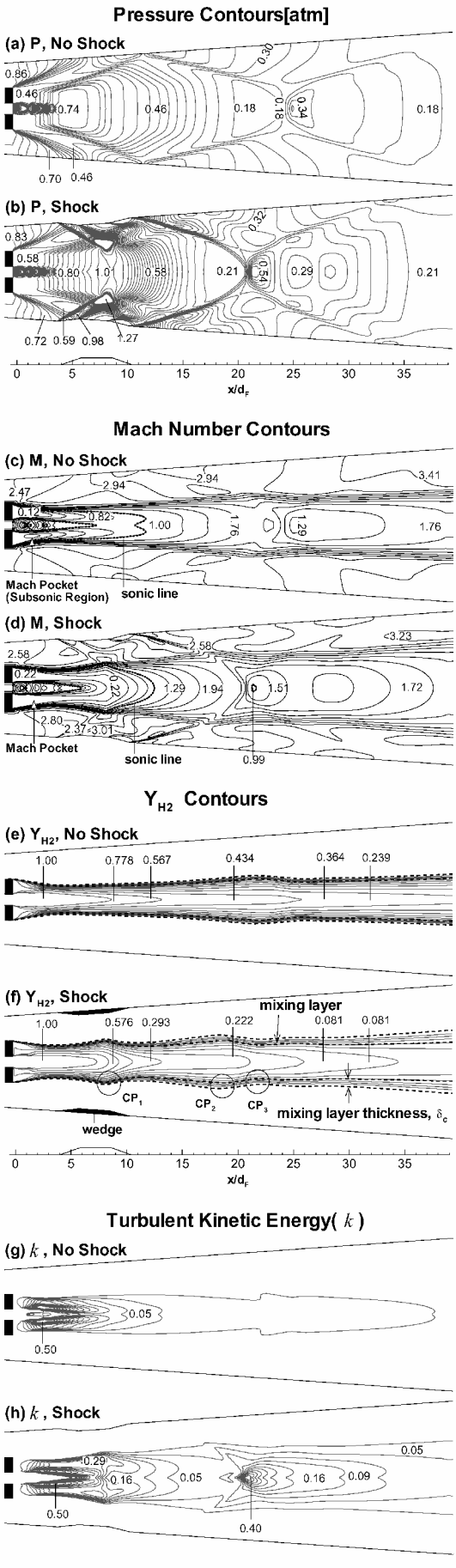

Fig. 3 Pressure, Mach number, Y_{H2}, and turbulent kinetic energy contours with combustion. In the case of a shock wave, the wedge is located at $4d_F$ ($x_W = 4d_F$).

Table 2 Crossing point position (reacting cases)

	Shock positions x_W/d_F					
Crossing point	0	1	2	3	4	8
CP_1	4	5	6	7	8	16
CP_2	14.5	15	16	17	18	26
CP_3	19	19.5	20	20.5	22	32

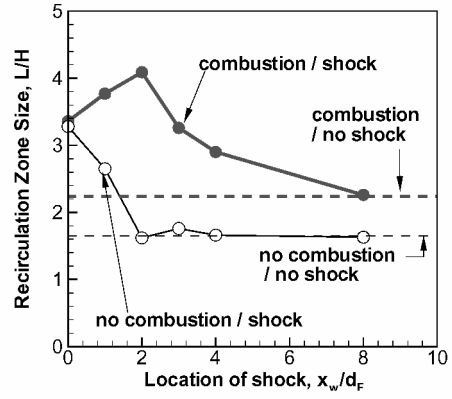

Fig. 4 Effects of shock waves on the size of recirculation zone (thickness of fuel nozzle lip $H = 0.92$ cm, $d_F = 0.70$ cm).

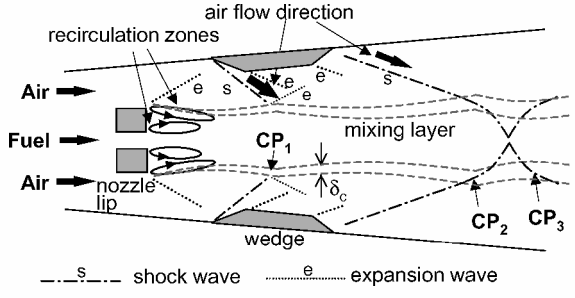

Fig. 5 Schemetic of the flowfield affected by the shock waves.

Effects of Shock Waves on Mixing

Figure 5 is a schematic of flowfields affected by the shock waves. The wedge mounted on the wall generates the shock waves, which interact with the mixing layer and the flame. Also, the shock wave changes the direction of the air flow toward the center, which may affect the size of the recirculation zone near the flame base and enhance the fuel–air mixing and the flame stability. The mixing layer thickness δ_c is defined as the distance between the line of $Y_{H2} = 4.25\%$ ($\phi = 1.5$) and the line of $Y_{H2} = 1.413\%$ ($\phi = 0.5$) on the basis of fuel concentration. In this computation area, there exist three crossing points (CPs) where interactions occur between the shock wave and the mixing layer, as shown in Fig. 5 (also see Fig. 3f). The strong/weak CPs are classified according to the increasing tendency of the growth rate of the mixing layer downstream of the shock waves. The strong interaction is observed at the first CP (CP_1), where the shock wave emerging from the leading edge of the wedge interacts with the upstream mixing layer. The relatively weak interaction is shown at the second and third CPs (CP_2 and CP_3), where the broadened downstream mixing layer interacts with the recompression shock wave issuing from the wall around the trailing edge of the wedge and reflected shock wave emerging from the centerline, respectively. The positions of CPs differ in each case. These values are listed in Table 2.

At CP_1, the shock wave reflects outward and then the shock wave is changed to the expansion wave; however, the mixing layer is deflected inward and immediately redirects outward again toward the downstream owing to the momentum of flowing gases. As a result, the growth rate δ_c' of the mixing layer thickness starts to increase significantly after CP_1, which indicates that mixing is

improved by the shock wave. However, at CP_2 and CP_3, the mixing layer is deflected by the shock wave. However, the shock wave is not reflected but refracted by the mixing layer. This is believed to be due to a smaller density gradient between fuel and air within the mixing layer than that of the first CP. Especially, it is noted that the growth rates at the second and third CPs are not so large as shown at the first CP. These are the different features between strong and weak interactions.

In compressible flows, development of the mixing layer is restrained by compressibility. The mixing layer enhancement by a shock wave is one of the effective methods. In this research, the effect of a shock wave is quantified by the measurement of mixing layer growth. Figure 6 shows the change in the mixing layer thickness in nonreacting and reacting cases. The mixing layer thickness is increased abruptly at the strong interaction point (CP_1), but the mixing layer growth rate is suppressed slightly at the weak interaction points (CP_2 and CP_3). The growth rate δ_c' of mixing layer thickness is increased by a factor of 3.3 to 4: i.e., it is varied from 0.02 to 0.08 in the nonreacting case and from 0.015 to 0.05 in the reacting case. The increased values of mixing layer growth rate δ_c' after a shock wave do not depend on the location where the shock wave and mixing layer interact.

Mixing can also be quantified by the plume penetration length, which is defined as the radial distance from the centerline to the edge of the mixing region, where the fuel mass fraction Y_{H2} is 0.5% (Ref. 18). Figure 7 shows the penetration trajectory, which is defined as the variation of the plume penetration length. It is noted that the peak value locations shown in Fig. 7 are almost matched to the CPs shown in Fig. 6. It is known that the fuel penetrates

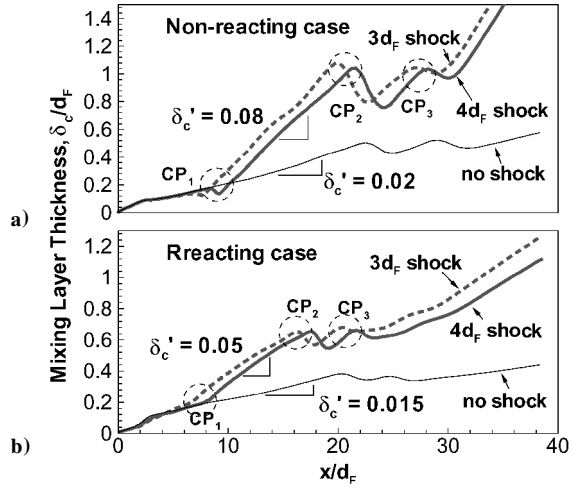

Fig. 6 Increase in mixing layer thickness after interaction with a shock wave.

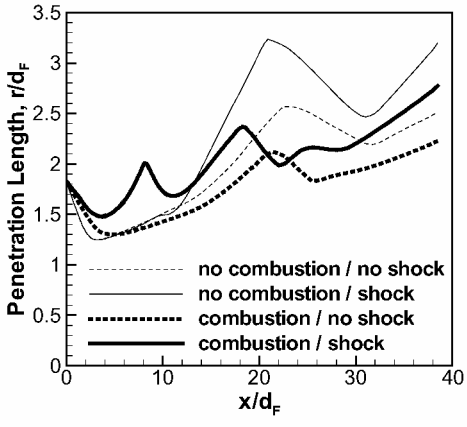

Fig. 7 Variation of plume penetration length. In the shock wave cases, the wedge is located at $x_w/d_F = 4$.

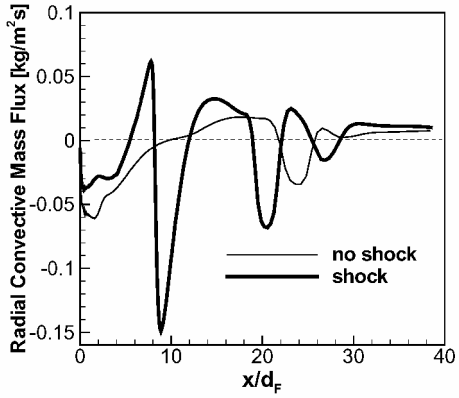

Fig. 8 Radial convective mass flux along the stoichiometric line in combustion.

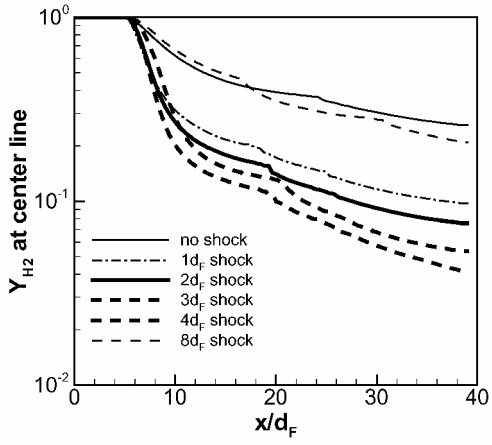

Fig. 9 Effect of shock wave location on the decay of centerline fuel mass fraction (no combustion case).

farther into the airstream in both the reacting and the nonreacting cases when the wedge-generated shock waves are present. This indicates that the mixing is enhanced due to the shock wave, which can be explained by the increase in the radial convective mass flux along the stoichiometric line, as shown in Fig. 8. The total inflows and outflows of mass flux are increased when the shock waves interact with the supersonic flame. In the shock wave/combustion case, the penetration trajectory appears to jump in the near-field region.

Figure 9 shows the decay of the fuel mass fraction along the centerline. This is the result of the nonreacting case. We found the same trend of fuel decay along the centerline in the reacting cases. However, the fuel decay in the reacting cases is influenced by not only the shock waves but also the fuel consumption due to the chemical reaction. Thus, we used the nonreacting case in the present study in order to see the effect of shock waves on the mixing with respect to the fuel decay. The location of the wedge is varied from 1 to $8d_F$ downstream of the fuel nozzle exit. It is shown that the shock waves cause intense mixing in the near-field recirculation region, as evidenced by the rapid decay of the fuel concentration between $x/d_F = 5$ and 10. With the proper location of the shock wave, the centerline fuel mass fraction is significantly decreased as compared with the no shock case. The decay of the fuel mass fraction is dependent on the location of the shock waves; as the shock wave is moved upstream properly toward the fuel nozzle, the fuel concentration is decreased more rapidly. Bryant and Driscoll[19] reported that the fuel concentration along the centerline disappeared within a distance of six times the fuel nozzle diameter when they performed the planar laser induced fluorescence (PLIF) measurement of acetone seeded into the fuel stream. It is certain that this rapid mixing in the near-field region has a strong effect on supersonic flame ignition and combustion.

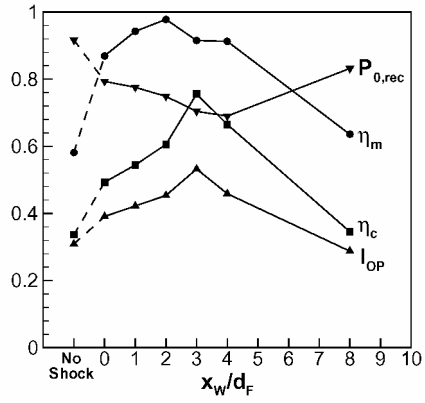

Fig. 10 Performance parameters for a model scramjet combustor by varying the location of shock waves within the computational domain up to $x = 38d_F$.

Performance Parameters of a Model Scramjet Combustor

Figure 10 shows the efficiencies of the model scramjet related to the position of the shock wave. The mixing efficiency, the combustion efficiency, the total pressure recovery, and the overall performance case are plotted. The mixing efficiency in the globally fuel-lean case is defined as described by Mao et al.[20]:

$$\eta_m(x) = \frac{\int \rho u Y_R dA}{(\int \rho u Y_F dA)_{x=0}} \tag{4}$$

where

$$Y_R = \begin{cases} Y_F, & Y_F < Y_{F,s} \\ Y_{F,s}(1 - Y_F)/(1 - Y_{F,s}), & Y_F > Y_{F,s} \end{cases}$$

Y_F and $Y_{F,s}$ denote a fuel mass fraction and a stoichiometric mass fraction of fuel, respectively. Y_R is the mass fraction of the least available reactant that reacts if complete reaction takes place without further mixing. It is noted that the overall mixing efficiency is over 90% for the shock case ($1 < x_W/d_F < 4$), whereas it is below 60% for the no shock case, which also indicates that the location of the shock wave has a strong effect on the mixing efficiency.

The combustion efficiency is a measure of the degree of completeness of the mixing and combustion and is defined as

$$\eta_c(x) = 1 - \frac{\int \rho u Y_F dA}{(\int \rho u Y_F dA)_{x=0}} = 1 - \frac{\dot{m}_F}{(\dot{m}_F)_{x=0}} \tag{5}$$

The combustion efficiency in the shock case of $x_W/d_F = 3$ is more than doubled compared with that of the no shock case. As a result, it is known that shock waves enhance the combustion of mixed reactants by increasing local pressure and temperature and by decreasing local velocity, which results in longer residence time.

The total pressure P_0 of incoming air and fuel is reduced by the viscous force in the boundary layer, flow separation, shock waves, fuel–air mixing, and combustion. The total pressure recovery $P_{0,\text{rec}}$ is defined as follows:

$$P_{0,\text{rec}}(x) = \frac{\int \rho u P_0 dA}{(\int \rho u P_0 dA)_{x=0}} \tag{6}$$

Then the total pressure loss is defined as $\Pi(x) = 1 - P_{0,\text{rec}}$. A value of $\Pi = 0$ indicates no total pressure loss. As expected, the total pressure recovery is decreased when shock waves are introduced into the flame. Also, the amount of total pressure recovery is very sensitive to the location of a shock-generating wedge. Hence, to evaluate the overall performance of a supersonic combustor, it is better to consider "mixing/combustion efficiency" and "total pressure loss" simultaneously.

Figure 10 shows that shock waves have a strong effect on the increase in the mixing and combustion efficiencies and that the two efficiencies have a similar trend. However, the increased total pressure loss is incurred inevitably despite the increased efficiencies of combustion and mixing in the presence of shock waves. To evaluate this tradeoff between enhanced combustion efficiency and decreased total pressure recovery, we introduced a new parameter, which is called the overall performance index, I_{op}:

$$I_{\text{op}} = \eta_c P_{0,\text{rec}} \tag{7}$$

Because the mixing efficiency is closely related to the combustion efficiency as shown in Fig. 10, we selected combustion efficiency as one of the important performance parameters. Also, the total pressure tends to decrease by the use of additional shock waves, although the mixing and combustion efficiency can be increased by the shock waves. Accordingly, we realized that the combustion efficiency and total pressure recovery should be considered simultaneously as important performance parameters in the present study.

It is found that the overall performance index is generally increased when the shock waves are added, even though the overall performance is the function of shock wave positions. This means that the combustor performance can be maximized when wedges are properly located in the combustor. The best result is obtained when 10-deg wedges are placed at the location of $x_W/d_F = 2$ to 4 in the present model combustor.

Conclusions

Shock wave effects are investigated numerically by changing shock position with particular emphasis on mixing efficiency, combustion efficiency, and total pressure loss of a supersonic hydrogen jet flame in a model scramjet combustor. The increase in the mixing layer is explained by the increase in mixing layer thickness. The major conclusions of the present study are as follows:

The shock waves are beneficial to the fuel–air mixing, especially in the near field of the fuel nozzle, as shown by the rapid increase in plume penetration length and by the rapid decay of fuel concentration on the centerline. This is believed to be due to the fact that the total inflows and outflows of mass flux are increased when the shock waves interact with a supersonic flame.

The flame-holding recirculation zone is elongated by a factor of 2 due to the shock waves behind the bluff body in the nonreacting case, which can be explained by the strong adverse pressure gradient caused by the shock wave near the recirculation zone. In the reacting case, the shock waves cause the further elongation of the recirculation zone due to the volumetric expansion of the combustible mixture. Hence, an upstream location of the shock wave is recommended to increase the size of the flame-holding recirculation zone.

In the presence of shock waves, the increase in total pressure losses is unavoidable despite the increased efficiencies of mixing and combustion. Hence, both the combustion efficiency and the total pressure loss should be considered simultaneously. Results show that the overall combustor performance can be maximized when the shock waves are properly located in the combustor.

Acknowledgments

The authors gratefully acknowledge the financial support provided under Grant 98-0200-04-01-3 from the Basic Research program of the Korea Science and Engineering Foundation and Grant M1-0104-00-0058 from the National Research Laboratory program of the Korea Institute of Science and Technology Evaluation and Planning.

References

[1]Marble, F. E., Hendricks, G. J., and Zukoski, E. E., "Progress Toward Shock Enhancement of Supersonic Combustion Process," AIAA Paper 87-1880, July 1987.

[2]Lu, P. J., and Wu, K. C., "On the Shock Wave Enhancement of Confined Supersonic Mixing Flows," *Physics of Fluids A*, Vol. 3, No. 12, 1991, pp. 3046–3062.

[3]Drummond, J. P., and Givi, P., "Suppression and Enhancement of Mixing in High-Speed Reaction Flow Fields," *Combustion in High-Speed Flow*, Kluwer Academic, Dordrecht, The Netherlands, 1994, pp. 191–229.

[4]Huh, H., and Driscoll, J. F., "Shock-Wave-Enhancement of the Mixing and the Stability Limits of Supersonic Hydrogen–Air Jet Flames," *Proceedings of the Combustion Institute*, Vol. 26, 1996, pp. 2933–2939.

[5]Choi, J.-Y., Jeung, I.-S., and Yoon, Y., "Numerical Study of Scram Accelerator Starting Characteristics," *AIAA Journal*, Vol. 36, No. 6, 1998, pp. 1029–1038.

[6]Choi, J. Y., Jeung, I. S., and Lee, S., "Dimensional Analysis of the Effect of Flow Conditions on Shock-Induced Combustion," *Proceedings of the Combustion Institute*, Vol. 26, 1996, pp. 2925–2932.

[7]Choi, J. Y., Jeung, I. S., and Yoon, Y., "Transient Simulation of the Superdetonative Model Ignition Process in SCRam Accelerator," *Proceedings of the Combustion Institute*, Vol. 26, 1996, pp. 2957–2963.

[8]Jachimowski, C. J., "An Analytical Study of the Hydrogen–Air Reaction Mechanism with Application to SCRamjet Combustion," NASA TP-2791, Feb. 1988.

[9]Menter, F. R., "Two-Equation Eddy-Viscosity Turbulence Models for Engineering Application," *AIAA Journal*, Vol. 32, No. 8, 1994, pp. 1598–1605.

[10]Wilcox, D. C., *Turbulence Modeling for CFD,* DCW Industries, La Cañada, CA, 1993.

[11]Bardina, J. E., Huang, P. G., and Coakly, T. J., "Turbulence Modeling Validation," AIAA Paper 97-2121, June 1997.

[12]Evans, J. S., and Schexnayder, C. J., Jr., "Influence of Chemical Kinetics and Unmixedness on Burning in Supersonic Hydrogen Flames," *AIAA Journal*, Vol. 18, No. 2, 1979, pp. 188–193.

[13]Moon, G.-W., Jeung, I.-S., and Choi, J.-Y., "Numerical Study of Thermal Choking Process in a Model Scramjet Engine," AIAA Paper 2000-3706, July 2000.

[14]Lee, B.-R., Moon, G.-W., Jeung, I.-S., and Choi, J.-Y., "Combustion of Thermal Choking Process in a Model Scramjet Engine," *Third Asia–Pacific Conference on Combustion*, Seoul, Republic of Korea, 2001, pp. 698–701.

[15]Huh, H., "An Experimental Study of Supersonic Hydrogen–Air Flames for SCRamjet Applications," Ph.D. Dissertation, Dept. of Aerospace Engineering, Univ. of Michigan, Ann Arbor, MI, 1996.

[16]Yoon, Y., Donbar, J. M., and Driscoll, J, "Blowout Stability Limits of a Hydrogen Jet Flame Within a Supersonic Heated, Coflowing Air Stream," *Combustion Science and Technology*, Vol. 97, No. 1–3, 1994, pp. 137–156.

[17]Winterfeld, G., "On the Burning Limits of Flame Holder Stabilized Flames in Supersonic Flow," CP34, Paper 28, AGARD, Aug. 1968.

[18]Fuller, R. P., Nejad, A. S., and Schetz, J. A., "Fuel Vortex Interactions for Enhanced Mixing in Supersonic Flow," *Journal of Propulsion and Power*, Vol. 14, 1998, pp. 135–145.

[19]Bryant, R. A., and Driscoll, J. F, "PLIF Images of Fuel Mixing and Flame Structure in a Supersonic Combustor," Work-in-Progress Session W4C17, Twenty-Seventh Symposium (International) on Combustion, Combustion Inst., Pittsburgh, PA, Aug. 1998.

[20]Mao, M., Riggins, D. W., and McClinton, C. R., "Numerical Simulation of Transverse Fuel Injection," NASA CR 1089, May 1990.

M. Sichel
Associate Editor